Lattice Boltzmann Simulations of Fluid Flows

Baochang Shi[1], Nangzhong He[1], Nengchao Wang[1], Zhaoli Guo[2], and Weibin Guo[1]

[1] Parallel Computing Institute,
Huazhong University of Science and Technology,
Wuhan 430074, People's Republic of China
sbchust@wuhan.cngb.com
[2] National laboratory of Coal Combustion,
Huazhong University of Science and Technology,
Wuhan 430074, People's Republic of China
pcihust@wuhan.cngb.com

Abstract. Our recent efforts focusing on improving the lattice Boltzmann method (LBM) are introduced, including an incompressible LB model without compressible effect, a flexible thermal LBM with simple structure for Bousinesq fluids, and a robust boundary scheme. We use them to simulate the lid-driven cavity flow at Reynolds numbers 5000–50000, the natural convection due to internal heat generation in a square cavity at Rayleigh number up to 10^{12}, respectively. The numerical results agree well with those of previous studies.

1 Introduction

Today, despite enormous progress in computational fluid dynamics (CFD), limitations still exist because of computer resources. It is apparent that several orders of magnitude improvement in both speed and memory are necessary to solve problems of contemporary interest. These requirements are obtained assuming today's solution algorithms and computer architecture. Since the technologies of scalar and vector computing have had substantial development, further work is unlikely to yield significant increases in computer performance. Massive parallel processing, on the other hand, appears to possess the capability to partially fill the gap between computational needs and present supercomputer performance. Although the supercomputer performance keeps rapid increase, it still could not satisfy the computational need in CFD due to the complex behavior of fluids, especially that of turbulence. Therefore, the efficient use of massively-parallel computers requires new algorithms with high performance. The lattice Boltzmann method (LBM) is a candidate of such algorithms [1-4].

The LBM is a relatively new approach that uses simple microscopic models to simulate complicated macroscopic behavior of transport phenomena. In recent years, the LBM method has achieved great success in simulations of fluid flows and modeling physics in fluids, involving complicated boundaries or/and complex fluids, such as turbulent flow, muti-phase/component fluids, free boundaries in flow systems, particle suspensions in fluid, reactive-diffusive systems and combustions,

X. Zhou et al. (Eds.): APPT 2003, LNCS 2834, pp. 322–332, 2003.

magnetohydrodynamics, crystal growing, granular flow and others [3,4]. Compared with the conventional CFD approach, LBM is simple to code, intrinsically parallel, ready for extending to three-dimensional problems and has clear physical pictures. It is also easy to incorporate complicated boundary conditions such as those in porous media.

The LB models commonly used in the solution of the incompressible Navier-Stokes (NS) equations can be viewed as compressible schemes to simulate incompressible fluid flows, and there is the compressible effect which might lead to some undesirable errors in numerical simulations. Some LB models have been proposed to reduce or eliminate such errors [5-7]. However, most of the existing LB models either can be used only to simulate steady flows or are still of artificial compressible form. So, when used to simulate unsteady incompressible flows, these methods require some additional conditions to neglect the artificial compressible effect. In Ref. [8], we have proposed a 9-bit incompressible LB model in two-dimensional space. To our knowledge, this model is the first one without compressible effect for simulating incompressible flows. The approach can be used in the solution of steady or unsteady problems and can also be used to develop other incompressible LB models in either two- or three-dimensional space.

In LBM simulations, boundary condition is a very important issue. Proper boundary conditions can reduce the computational cost and enhance the numerical stability of algorithms. At solid walls, the original schemes are realized by particle density bounce-back. These bounce-back conditions are simple and can be used to some flow problems with complex geometries. But it is known that bounce-back wall boundary conditions are of first-order accuracy, and can not process the complex boundary conditions. To avoid of these problems, several new type boundary-processing schemes have been proposed and improved the overall accuracy of LB methods [9]. But, these schemes are imposed certain restrictions. Although the extrapolation scheme proposed by Chen *et al*. used second-order extrapolation, which is consistent with LBM, we found that the second-order extrapolation scheme has poor stability for high Reynolds numbers. It is necessary to establish a processing scheme for boundary conditions, which is of higher order accuracy, has robust stability and is efficient for arbitrary complex geometric boundaries.

In the present paper, our recent efforts focusing on above problems are introduced, including an LBM without compressible effect, a flexible thermal LBM with simple structure for Bousinesq fluids, and a robust boundary scheme. We use them to simulate the lid-driven cavity flow at Reynolds numbers 5000-50000, and the natural convection due to internal generation in a square cavity at Rayleigh number up to 10^{12}, and Prandtl number 0.25 and 0.6. The numerical results agree well with those of previous studies.

2 Background of Lattice Boltzmann Method

2.1 Lattice Boltzmann Method

A popular LB model is the so-called lattice BGK model (LBGK) with the single relaxation time approximation [3] :

$$f_i(\mathbf{x}+c\mathbf{e}_i\Delta t,t+\Delta t)-f_i(\mathbf{x},t)=-\tau^{-1}[f_i(\mathbf{x},t)-f_i^{(eq)}(\mathbf{x},t)], \tag{1}$$

where $\mathbf{e}_i$ is the discrete velocity direction, and $c=\Delta x/\Delta t$ is particle speed, Δx, Δt, and τ are the lattice grid spacing, the time step and the dimensionless relaxation time, respectively. $f_i(\mathbf{x},t)$ is the distribution function at node $\mathbf{x}$ and time t with velocity $\mathbf{e}_i$, and $f_i^{(eq)}(\mathbf{x},t)$ is the corresponding equilibrium distribution depending the lattice model used. The nine-bit square lattice model referred to as D2Q9 model has been successfully used for simulating 2-D flows. For the D2Q9 model, $\mathbf{e}_i$ is defined as

$\mathbf{e}_0=\mathbf{0}$, $\mathbf{e}_i=(\cos[(i-1)\pi/2],\sin[(i-1)\pi/2])$ for i=1:4,

$\mathbf{e}_i=\sqrt{2}(\cos[(i-5)\pi/2+\pi/4],\sin[(i-5)\pi/2+\pi/4])$ for i=5:8.

The equilibrium distribution for the D2Q9 model is in the form of

$$f_i^{(eq)}=\omega_i\rho[1+3\frac{(\mathbf{e}_i\cdot\mathbf{u})}{c}+4.5\frac{(\mathbf{e}_i\cdot\mathbf{u})^2}{c^2}-1.5\frac{|\mathbf{u}|^2}{c^2}]\triangleq\omega_i\rho[1+s_i(\mathbf{u})], \tag{2}$$

where ω_i is the weighting factor given by $\omega_0=4/9$, $\omega_i=1/9(i=1:4)$, $\omega_i=1/36(i=5:8)$.

The flow density, momentum fluxes and kinetic viscosity can be evaluated as

$$\rho=\sum_{i=0}^{8}f_i,\ \rho\mathbf{u}=\sum_{i=1}^{8}c\mathbf{e}_i f_i,\ \upsilon=(\tau-1/2)c_s^2\Delta t, \tag{3}$$

where $c_s=c/\sqrt{3}$ is the speed of sound in this model and the equation of state is that of an idea gas, $p=c_s^2\rho$.

Through multi-scaling expansion, the incompressible NS equation can be derived to the second order under the low Mach number limitation [3]:

$$\partial_t\rho+\nabla\cdot(\rho\mathbf{u})=0, \tag{4}$$

$$\partial_t(\rho\mathbf{u})+\nabla\cdot(\rho\mathbf{u}\mathbf{u})=-\nabla p+\upsilon\nabla\cdot(\nabla\rho\mathbf{u}+\nabla(\rho\mathbf{u})^T). \tag{5}$$

From Eqs.(4)-(5), we can see that the LBM is in fact an artificial compressible scheme for the incompressible NS equation. This may lead to compressible effect. We recently proposed a true incompressible LBGK model (ILBGK) for the incompressible NS equation without compressible effect [8]. The equilibrium distribution in ILBGK is defined by

$$f_i^{(eq)}=\lambda_i p+s_i(\mathbf{u}), \tag{6}$$

where $\lambda_0=-4\sigma/c^2$, $\lambda_i=\lambda/c^2$ (i=1:4) and $\lambda_i=\gamma/c^2$ (i=5:8) with parameters σ,λ, and γ satisfying $\lambda+\gamma=\sigma$, $\lambda+2\gamma=1/2$, and $s_i(\mathbf{u})$ as in Eq.(2).

The flow velocity, pressure and kinetic viscosity are given by

$$\mathbf{u}=\sum_{i=1}^{8}c\mathbf{e}_i f_i,\ p=\frac{c^2}{4\sigma}[\sum_{i=1}^{8}f_i+s_0(\mathbf{u})],\ \upsilon=(\tau-1/2)c_s^2\Delta t.$$

The ILBGK is a second order scheme for true incompressible NS equation,

$$\nabla \cdot \mathbf{u} = 0\,, \tag{7}$$

$$\partial_t\, \mathbf{u} + \mathbf{u} \cdot \nabla \mathbf{u} = -\nabla p + \upsilon \nabla^2 \mathbf{u}\,. \tag{8}$$

2.2 Boundary Conditions

We have found that most of the existing boundary schemes commonly used in LBGK usually encounter numerical instability for flows at large *Ra* or *Re*. In a previous study we developed a non-equilibrium extrapolation rule for velocity and pressure boundary condition [10], which is of second order, simple form, and exhibits much better numerical stability. This rule is based on the decomposition of distribution function:

$$f_i(\mathbf{x}_b, t) = f_i^{(eq)}(\mathbf{x}_b, t) + f_i^{(neq)}(\mathbf{x}_b, t)\,, \tag{9}$$

where $f_i^{(neq)}$ is the non-equilibrium part of f_i, $\mathbf{x}_b$ is a node on boundary.

For velocity boundary, we have

$$f_i(\mathbf{x}_b, t) = \bar{f}_i^{(eq)}(\mathbf{x}_b, t) + (f_i(\mathbf{x}_f, t) - f_i^{(eq)}(\mathbf{x}_f, t))\,, \tag{10}$$

while for pressure boundary, we use

$$f_i(\mathbf{x}_b, t) = \bar{\bar{f}}_i^{(eq)}(\mathbf{x}_b, t) + (f_i(\mathbf{x}_f, t) - f_i^{(eq)}(\mathbf{x}_f, t))\,, \tag{11}$$

where

$$\bar{f}_i^{(eq)}(\mathbf{x}_b, t) = \lambda_i p(\mathbf{x}_f, t) + s_i(\mathbf{u}(\mathbf{x}_b, t))\,,\quad \bar{\bar{f}}_i^{(eq)}(\mathbf{x}_b, t) = \lambda_i p(\mathbf{x}_b, t) + s_i(\mathbf{u}(\mathbf{x}_f, t))\,,$$

$\mathbf{x}_f$ is its nearest neighbor fluid node of $\mathbf{x}_b$.

3 Numerical Results

3.1 Lid-Driven Cavity Flow

The configuration of the lid-driven cavity flow considered in this paper consists of a two-dimensional square cavity whose top plate moves from left to right with a uniform velocity (*U*=1, here), while the other three walls are fixed. The flow is described by the dimensionless incompressible NS equations, that is Eqs.(7)-(8), where $\mathbf{u} = (u, v)$ is the velocity vector, p is the pressure, and $\upsilon = 1/Re$ is the kinetic viscosity, *Re* the Reynolds number.

Numerical simulations were carried out using the methods presented above for the driven cavity flow with *Re*=5000, 7500, 10000, 15000, 20000, and 50000, respectively, on 256×256 lattice. The relaxation parameter $\omega = \tau^{-1}$ is set to be 1.85, 1.92, 1.95, 1.95, 1.96 and 1.985, respectively. $(\sigma, \lambda, \gamma)$ in Eq.(6) is set to be $(5/12, 1/3, 1/12)$ such that $(\lambda, \gamma) = 3\times(\omega_1, \omega_5)$ which has the symmetry to agree with the

method, and we find that the simulations with this set are more robust. For the walls, no-slip boundary conditions were prescribed by the non-equilibrium extrapolation method given above. The flow with *Re*=5000 is first simulated, where the initial condition is set as $p = 0$, and the velocities at all nodes, except the top nodes, are set as $u = v = 0$. The simulations for higher *Re* start from the solution obtained for lower *Ra* as initial condition. In the simulations, steady solutions are obtained for $Re \le 10^4$. For $Re=1.5\times10^4$, the flow becomes periodic, and a period is about 2000 time step. For $Re=2\times10^4$ and 5×10^4, the flow becomes unsteady, and the solutions at 300000 and 350000 time steps are given, respectively.

Fig. 1. shows the contours of the stream function of the flows for the Reynolds numbers considered. These plots show clearly the effect of the Reynolds number on the flow pattern. At *Re*=5000, in addition to the primary, center vortex, and three first-class vortices, a pair of secondary ones of much smaller strength develop in the lower corners of the cavity. When Reynolds number reaches to 7500, a tertiary vortex appears in the lower right corner. Stationary solutions were found for Reynolds numbers up to 10000. We can also see that the center of the primary vortex moves toward the geometric center of the cavity as the Reynolds number increases and becomes fixed in *x*-direction. As the Reynolds number increases, no more steady solution was found and the flow becomes periodic in time at *Re*=15000. Here streamlines in one period for *Re*=15000 are plotted in Fig. 2. As the Reynolds number increases to 20000, the period begins to be broken, but the primary vortex is still stable. When *Re* reaches 50000, the flow becomes chaos and the primary vortex is unsteady and broken. To quantify the results, the locations of the vortex are listed in Table 1. From the table, we can see that these values predicted by the LBGK method agree well with those of previous work [2,11,12].

3.2 Natural Convection Flow with Internal Heat Generation

Natural convection (NC) in enclosures is a classical problem in the heat transfer literature and serves as one of the most popular test-problems for numerical methods for incompressible viscous flows. Much more work has addressed two main classes of NC flows, those heated from below and those from side [13,14]. Although NC due to internal heat generation is not less important, it drew much less attention in the past than the two classes above. However, in recent years, it becomes a subject of intense interest mainly due to nuclear safety issues [15,16]. Horvat *et al*. recently simulated the NC flows with internal heat generation in a square cavity for a wide range of *Ra* and Prandtl numbers (*Pr*): *Ra* 10^6-10^{13} and *Pr* 0.25-8 by using the LES method [15,16]. Since the NC flows at large *Ra* have complex behavior, the solution of them is very difficult. Efficient methods are still needed for further study, especially for 3D problems. The LBGK method is perhaps a suitable one.

The flow considered is in an enclosure of height *H* and width *W* (aspect ratio $A = H/W$), and governed by two-dimensional unsteady Boussinesq equations in primitive variables[15]. Since the force or source terms in momentum and temperature are required to be of order $O(\Delta t)$ in LBGK, where Δt is the time step, we use the following dimensionless equations in the paper by setting $\mathrm{U} = Ra^{0.5}\mathbf{u}$, $t' = Ra^{-0.5}t$, and $P = pRa$ in the dimensionless equations for the flow in Ref.[15]:

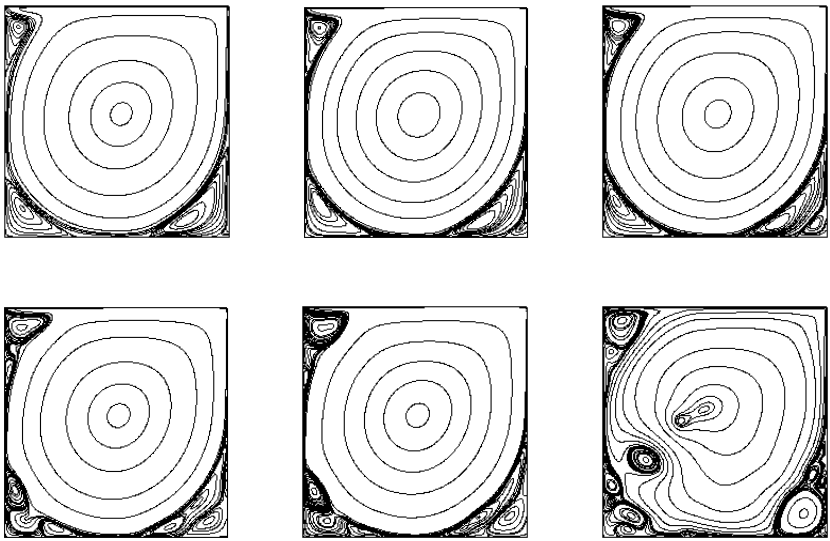

Fig. 1. Streamlines of the flow at: *Re*=5000, 7500, 10000 (Top: left to right), and *Re*=15000, 20000, 50000 (Bottom: left to right)

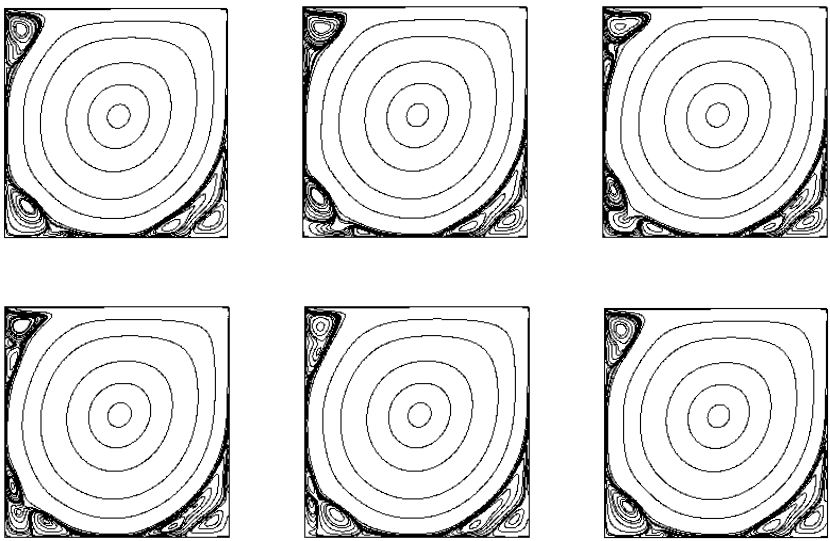

Fig. 2. Streamlines of the flow at *Re*=15000 in one period from 155000 to 157000 time steps; T=1.9560

Table 1. Locations of Vortex of the Driven Cavity Flow. The letters T, B, L, and R denote top, bottom, left, and right, respectively; a. Ghia *et al*.[11]; b. Hou and Zhou [2]; c. Present work

Re		Primary	First (T)	First (BL)	First (BR)	Second (BL)	Second (BR)
5000	a	0.5117, 0.5352	0.0625, 0.9102	0.0703, 0.1367	0.8086, 0.0742	0.0117, 0.0078	0.9805, 0.0195
	b	0.5176, 0.5373	0.0667, 0.9059	0.0784, 0.1373	0.8078, 0.0745	-	-
	c	0.5156, 0.5352	0.0625, 0.9063	0.0742, 0.1328	0.8086, 0.0742	0.0039, 0.0039	0.9961, 0.0742
7500	a	0.5117, 0.5322	0.0664, 0.9141	0.0645, 0.1504	0.7813, 0.0625	0.0117, 0.0117	0.9492, 0.0430
	b	0.5176, 0.5333	0.0706, 0.9098	0.0706, 0.1529	0.7922, 0.0667	-	-
	c	0.5156, 0.5352	0.0664, 0.9102	0.0664, 0.1484	0.7930, 0.0664	0.0078, 0.0039	0.9961, 0.0742
10000	a	0.5117, 0.5333	0.0703, 0.9141	0.0586, 0.1641	0.7656, 0.0586	0.0156, 0.0195	0.9336, 0.0625
	c	0.5117, 0.5313	0.0703, 0.9102	0.0625, 0.1563	0.7813, 0.0625	0.0117, 0.0117	0.9492, 0.0625
15000	c	0.5117, 0.5313	0.0781, 0.9141	0.0547, 0.1992	0.7227, 0.0391	-	0.9219, 0.0781
20000	c	0.5117, 0.5273	0.0820, 0.9102	0.0703, 0.1758	0.7109, 0.0391	-	0.8672, 0.0742

$$\nabla \cdot \mathbf{u} = 0\,, \tag{12}$$

$$\partial_t\, \mathbf{u} + \mathbf{u} \cdot \nabla \mathbf{u} = -\nabla p + \upsilon \nabla^2 \mathbf{u} + Pr\Theta \mathbf{k}\,, \tag{13}$$

$$\partial_t\, \Theta + \mathbf{u} \cdot \nabla \Theta = D\nabla^2 \Theta + D\,, \tag{14}$$

where $\upsilon = PrRa^{-0.5}$, $D = Ra^{-0.5}$, $\mathbf{k}$ is the unit vector in the *y*-direction, *Pr* is the Prandtl number and *Ra* the Rayleigh number; t', $\mathbf{U}$, *P* and Θ are the dimensionless time, velocity vector, pressure and temperature, respectively, as in Ref.[15].

The boundary conditions are taken to be $\mathbf{u} = 0$ and $\Theta = 0$ on all the four walls; Here we set $A = 1$. At the beginning of the simulation, the fluid was considered at rest and isothermal, with mean temperature $\Theta = 0$. Thus the initial conditions are set to be $\mathbf{u} = 0, \Theta = 0$ for all cases.

We first modify the ILBGK model described by Eqs.(1) and (6) for the velocity field by adding a term to the evolution equation:

$$f_i(\mathbf{x} + c\mathbf{e}_i\Delta t, t + \Delta t) - f_i(\mathbf{x}, t) = -\tau^{-1}[f_i(\mathbf{x}, t) - f_i^{(eq)}(\mathbf{x}, t)] + F_i\Delta t\,,$$

where $F_i = \dfrac{Pr}{2c}\alpha_i \mathbf{e}_i \cdot \mathbf{k}\Theta$ such that $\sum_{i=1}^{8} ce_i F_i = Pr\Theta k$, and $\alpha = \delta_{i2} + \delta_{i4}$. Other forms of F_i can also be used.

To solve Eq. (14), we utilize a D2Q5 lattice consisted of $\mathbf{e}_i$ $(i = 0:4)$ as used in Eq. (1), and the LBGK equation for Eq. (14) reads

$$\Theta_i(\mathbf{x} + c\mathbf{e}_i\Delta t, t + \Delta t) - \Theta_i(\mathbf{x}, t) = -\tau_\Theta^{-1}[\Theta_i(\mathbf{x}, t) - \Theta_i^{(0)}(\mathbf{x}, t)] + T_i\Delta t\,, \tag{15}$$

where $\Theta_i^{(0)} = (\Theta/5)[1+2.5(\mathbf{e}_i \cdot \mathbf{u})/c]$ is the equilibrium, and for the source term we take $T_i = (D/5)[1+2.5(\mathbf{e}_i \cdot \mathbf{u})/c]$ such that $\sum_{i=0}^{4} T_i = D$. Θ and D are calculated by

$$\Theta = \sum_{i=0}^{4} \Theta_i \ , \ D = (2\tau_\Theta - 1)(\Delta x)^2 / (5\Delta t) \ . \tag{16}$$

It should be noted that the other lattices could also be used for Eq. (14). However, the lattice introduced here is the simplest one with rest particle. Note that in Ref. [17] we successfully simulated the NC flow heated from side (without heat source in Eq.(14)) at *Ra* up to 10^{10} using a D2Q4 model for Eq. (15) without the source term. It was found that the TLBGK with D2Q5 has better numerical stability than that with D2Q4 for the flows considered here.

Similarly, for thermal boundary condition, we use

$$\Theta_i(\mathbf{x}_b, t) = \Theta_i^{(0)}(\mathbf{x}_b, t) + (\Theta_i(\mathbf{x}_f, t) - \Theta_i^{(0)}(\mathbf{x}_f, t)) \ . \tag{17}$$

We simulate the flow with *Ra*=10^6-10^{11} for *Pr*=0.25 and *Ra*=10^6-10^{12} for *Pr*=0.60 respectively, based on a 256×256 uniform lattice. The corresponding relaxation parameter $\omega = \tau^{-1}$ is set to be 0.90-1.991 for the case *Pr*=0.60, and 1.30-1.987 for *Pr*=0.25, while τ_Θ is given by Eq. (16). In the simulations, steady solutions for *Ra*=10^6 and 10^7 were reached. For *Ra*=10^8-10^{12}, the flow becomes unsteady, and solutions were obtained from 10^5 to 4.0×10^5 time steps, corresponding to the dimensionless time $t' \approx 0.1$, 0.5, 0.03, 0.015 and 0.01, respectively, as in Ref. [15]. It is well known that the numerical stability of the LBGK models is usually very poor as $\omega = \tau^{-1} \to 2$. While we found that our scheme was still stable and accurate even as $\omega = 1.991$, at which the computation blows up using other schemes for the velocity and temperature boundary conditions.

Isotherms of the flows are shown in Fig.3. From the figures, we can see that the main features of the flows are in agreement with those obtained in Ref. [15]. To quantify the results, the time-boundary-averaged Nusselt numbers (Nu_{ave}) obtained by the TLBGK and those in Ref.[15] are plotted in Fig.4-5 ($\log_{10}$-$\log_{10}$ diagram). It can be found that our results for $Ra \le 10^9$ agree well with those in Ref.[15], while the others are different a little, which is perhaps due to the different methods used.

4 Conclusion

We proposed the LBGK models with a robust boundary scheme for complex flows at large *Re* or *Ra*. The numerical results agree well with those of previous studies. Since little work on simulations of flows at large *Re* or *Ra* by LBM was performed before, our work is important for the development of LBM. The proper implementation of the boundary conditions is crucial for the LBGK simulation. Non-equilibrium extrapolation method has robust stability and the overall accuracy of distribution function is of second order. With the proposed boundary schemes, we can simulate the flow at very large *Re* or *Ra*. We found that other LBGK models with these boundary schemes have also better stability. It is also found that if a finer lattice is

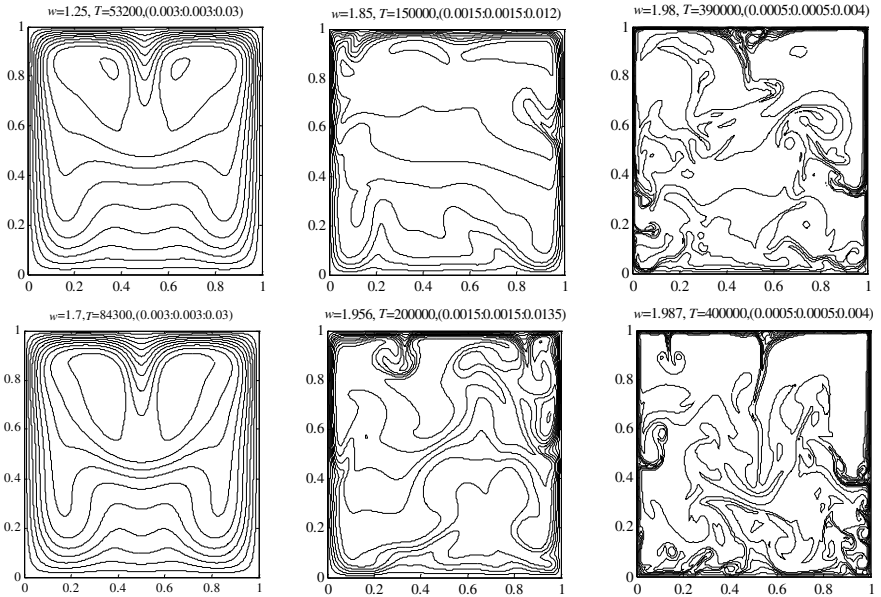

Fig. 3. Temperature isotherms: Pr=0.6 (top) and Pr=0.25 (bottom). Ra=10^7, 10^9, 10^{11} from left to right. The data listed above each subfigure are the relaxation parameter ω, time steps T, and values of temperature isotherms

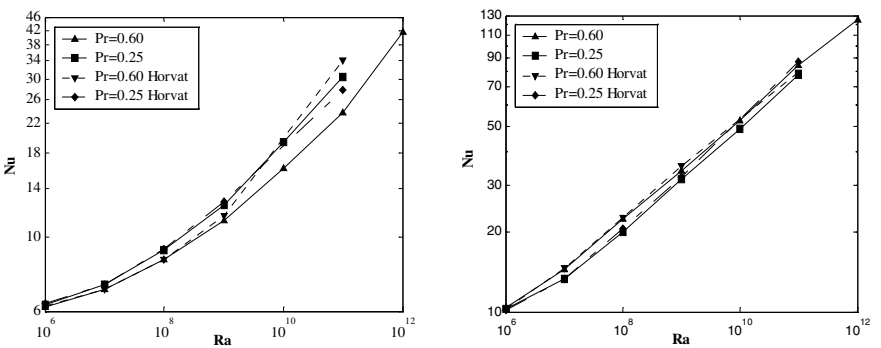

Fig. 4. Rayleigh number vs. time-boundary-averaged Nusselt number on the bottom(left) and side(right) boundaries

used, flows at larger Re or Ra than those here can be simulated using the present models. Moreover, our models can be easily extended to 3D problem. LBGK method is a relatively new approach for simulating complex flows. It is parallel in nature due to the locality of particle interaction and the transport of particle information, so it is well suited to massively parallel computing. Applying LBM to other complex flows is challenging work.

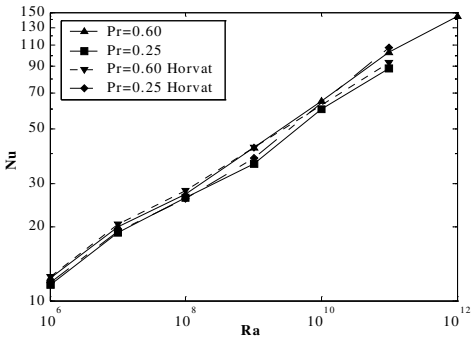

Fig. 5. Rayleigh number vs. time-boundary-averaged Nusselt number on the top boundary

Acknowledgments. This work is supported by the National Natural Science Foundation of China under Grant Nos. 60073044 and 70271069, and the State Key Development Programme for Basic Research of China under Grant No. G1999022207.

References

1. Frish, U., d'Humiéres, D., Hasslacher, B., Lallemand, P., Pomeau, Y., Rivet, J.-P.: Lattice gas hydrodynamics in two and three dimensions, Complex Syst. 1 (1987) 649–707
2. Hou, S., Zou, Q., Chen, S., Doolen, G., Cogley, A.C.: Simulation of cavity flow by the lattice Boltzmann method, J. Comput. Phys. 118 (1995) 329–347
3. Chen S., Doolen G.: Lattice Boltzmann method for fluid flows, Annu. Rev. Fluid Mech. 30 (1998) 329–364
4. Luo, L.-S.: The lattice–gas and lattice Boltzmann methods: past, present, and future, Proc. Int. Conf. Applied CFD, (2000) 52–83
5. He X., Luo L.-S.: Lattice Boltzmann model for the incompressible Navier-Stokes equation, J. Stat. Phys. 88 (1997) 927–944
6. Lin, Z., Fang, H., Tao, R.: Improved lattice Boltzmann model for incompressible two-dimensional steady flows, Phys. Rev. E. 54 (1997) 6323–6330
7. Zou, Q., Hou, S., Chen, S., Doolen, G.: An improved incompressible lattice Boltzmann model for time-independent flows, J. Stat. Phys. 81 (1995) 35–48
8. Guo, Z., Shi, B., Wang, N.: Lattice BGK model for incompressible Navier-Stokes equation, J. Comput. Phys. 165 (2000) 288–306
9. Maier, R.S., Bemard, R.S., Grunau, D.W.: Boundary conditions for the lattice Boltzmann method, Phys. Fluid. 8 (1996) 1788–1801
10. Guo, Z., Zheng C., Shi, B.: An extrapolation method for pressure and velocity boundary conditions in lattice Boltzmann method, Chin. Phys. 11 (2002) 366–374
11. Ghia, U., Ghia, K.N., Shin, C.T.: High-Re solutions for incompressible flow using the Navier-Stokes equations and a multigrid method, J. Comput. Phys. 48 (1982) 387–411
12. Schreiber, R., Keller, H.: Driven cavity flow by efficient numerical techniques, J.Comput.Phys.49 (1983) 310
13. de V. Davis, G.: Int. J. Numer. Methods Fluids. 3 (1983) 249

14. Xin, S., Le Quéré, P.: Direct numerical simulations of two-dimensional chaotic natural convection in a differentially heated cavity of aspect ratio 4, J. Fluid Mech. 304 (1995) 87–118
15. Horvat, A., Kljenak, I., Marn, J.: Int. J. Heat Mass Transfer. 44 (2001) 3985–3995
16. Horvat, A.: PhD Thesis, University of Ljubljana, Slovenia, (2001)
17. Shi, B., Guo Z., Wang, N.: LBGK Simulations of Turbulent Natural Convection in a Cavity, Chin. Phys. Lett. 19 (2002) 515–517